IEEE Access
Multidisciplinary | Rapid Review | Open Access Journal

Received July 18, 2019, accepted July 26, 2019, date of publication August 7, 2019, date of current version August 28, 2019.

Digital Object Identifier 10.1109/ACCESS.2019.2933694

Double-Loop Wavefront Tilt Correction for Free-Space Quantum Key Distribution

ALEJANDRO OCAMPOS-GUILLÉN, JORGE GÓMEZ-GARCÍA, NATALIA DENISENKO, AND VERONICA FERNANDEZ

Institute of Physical and Information Technologies, Spanish National Research Council (CSIC), 28006 Madrid, Spain

Corresponding author: Veronica Fernandez (veronica.fernandez@iec.csic.es)

This work was supported in part by the *Ministerio de Economía y Competitividad* (MINECO /FEDER, UE), *Fondo Social Europeo* (FSE) through the *Programa Operativo de Empleo Juvenil* under Grant TEC2015-70406-R, in part by the Comunidad de Madrid, Spain, through the Project CYNAMON under Grant P2018/TCS-4566, in part by the Co-Financed with FSE and Fondo Europeo de Desarrollo Regional (FEDER) European Union (EU) Funds, and in part by the CSIC Research Platform on Quantum Technologies under Grant PTI-001.

ABSTRACT Both free-space and optical fiber quantum key distribution (QKD) links will coexist in future quantum networks, requiring efficient coupling between both types of channels. However, wavefront distortions introduced by the atmospheric channel can severely affect this efficiency. Active mechanisms such as precise beam tracking or steering can correct for some of these wavefront distortions, considerably improving the signal-to-noise ratio of the received quantum signal in many scenarios. A tracking system that uses two, instead oftypically one, controlling loops for tilt correction, stabilizes the beam in the whole optical axis of the receiver relaxing the restrictions of the receiver's optical design, and reduces the area of beam fluctuations in the receiver's focal plane a 24% more than a single-loop configuration. The tracking system was characterized in a QKD system at a 300 meter-link in moderate to strong turbulent conditions ($C_n^2 - 10^{-14} - 10^{-13}\mathrm{m}^{-2/3}$) and an improved coupling efficiency of a factor of 2.1 and 1.6 was obtained for a 9.5 μm-core diameter standard telecommunications Single Mode Fiber (SMF) and a 25 μm-core diameter multimode fiber (MMF), respectively. This reduces the quantum bit error rate (QBER) caused by solar background photons in a 52 % for the former and 39% for the latter, enabling an increase in the secret key rate ofmore than one order ofmagnitude for SMF and a factor of five for MMF. These results are promising for enabling QKD free-space links and their interconnection to fiber optic infrastructure in realistic scenarios of communication networks of high turbulence regimes and daylight conditions.

INDEX TERMS Quantum key distribution, beam steering, beam tracking, free-space quantum communication, quantum cryptography, wavefront tilt correction.

I. INTRODUCTION

Recent research in free-space Quantum Key Distribution (QKD) has focused on increasing the feasibility of practical systems in real scenarios, which implies fulfilling several challenges like increasing the key rate, the propagating distance and making practical systems compact, robust, and low cost [1]–[7]. Many advances on stationary links have been reported in the last few years [8]–[11], whereas other potential scenarios for mobile systems, such as aircrafts [12], hot-air balloons [13] and Unmanned Aerial Vehicles (UAVs) [14] have also been explored. In addition, after several tests and proofs to analyze their possibilities, links involving satellites have also been recently demonstrated [15]–[18].

The associate editor coordinating the review of this article and approving it for publication was Wei Huang.

Future wireless networks will use different types of communicating channels depending on their functionality [19]. Some will include only wireless links, such as in cases of communication among small-sized satellites, high altitude platforms and UAVs, whereas others will also include fiber channels, such as in cases where communication must be sent to a ground station or relayed to a fiber-optic network. In the latter case the interconnection among both types of transmission channels, air and fiber, must be optimized to avoid signal losses. This optimization includes techniques for reducing the effects of atmospheric turbulence [20], [21] through beam steering/tracking [22], [23] and adaptive optics [24], [25]. However, tracking systems including both types of correction usually require bulky and costly equipment. Considering that potential applications will likely involve networks with many users a solution that it is both simple and cheap is desired.

Therefore, it is interesting to assess quantitatively ifwavefront tilt correction alone is capable of enabling successful free-space QKD in realistic scenarios, such as those characterized by high turbulent regimes and daylight scenarios. After all, correcting tilt accounts for reducing the distortion of the wavefront in an 86% [20].

Beam tracking systems typically use one control loop, enabling correction in a single plane of the optical axis. Using two instead of one control loop stabilizes the beam in the whole optical axis of the receiver, and the planes where the correction can be observed are infinite. This facilitates the optical design by removing the constraint of using specific planes where detectors or other optical components must be placed with high precision. In this work, we present a double-loop tilt-correcting system and its characterization through the decrease in the receiver's beam focal area and its effect on the quantum bit error rate (QBER) and secret key rate (SKR) of a QKD system.

The structure of the article is organized as follows. Section II briefly introduces some theoretical parameters to quantify atmospheric turbulent effects in optical links. Section III describes the experimental setup of the double-loop tilt- correcting system. Section IV shows the experimental results in terms ofreduction ofbeam fluctuations at the focal plane of the receiver, increased coupling efficiency in optical fiber, QBER reduction and increase in SKR. Finally, in section V conclusions and future work are discussed.

II. CHARACTERIZING ATMOSPHERIC TURBULENCE IN AN OPTICAL SYSTEM

Atmospheric turbulence distorts the wavefront of a propagating laser beam giving rise to effects such as'dancing' of the beam center (beam wandering); spreading of the beam beyond normal diffraction (beam spreading); and random fluctuations of the irradiance (scintillation) and phase. These effects can be modeled as classical optical aberrations [26] whereby lower-order aberrations represent displacements of the beam centroid from the center of the propagating path, *i.e.*, a *tilt* movement in the x and y directions.

This tilt changes the angle of arrival of the optical beam upon receival, which, at the focal plane, are translated into spatial displacements of the beam centroid known as *spot focal wander*, r_a, given usually by the *root-mean-square* (*rms*) value $\sqrt{\langle r_a^2 \rangle}$.

Likewise, the angle of arrival, also known as *tilt angle* θ_{tilt} is obtained from dividing r_a by the effective focal length f_{eff} of the receiver system [20]:

$$\sqrt{\left\langle \theta_{tilt}^2 \right\rangle} = \frac{\sqrt{\left(r_a^2\right)}}{f_{eff}} \tag{1}$$

θ_{tilt} defines the (semi angle) field of view of the aperture of radius r_a placed in the focal plane of the receiver. According to the beam propagation theory, when using the Kolmogorov spectrum, atmospheric turbulences can be classified through the refractive-index structure parameter C_n^2. This parameter can be calculated through the link distance (L), the beam diameter of the receiver aperture ($2w_G$),[1] and the tilt angle $\langle \theta_{tilt}^2 \rangle$, using the following equation [20]:

$$C_n^2 = \frac{\left\langle \theta_{tilt}^2 \right\rangle}{2.91L\,(2w_G)^{-1/3}} \tag{2}$$

Atmospheric turbulence conditions range from values of C_n^2 of $10^{-17}\mathrm{m}^{-2/3}$ or less, when the turbulence is considered ''weak'', to values equal or larger than $10^{-13}\mathrm{m}^{-2/3}$, when the values are considered''strong''[20]. The values in between are considered as ''moderate'' turbulence.

Another classification of the turbulent conditions is through the *Rytov* parameter σ_R. Assuming a Gaussian-beam wave arriving at the receiver, σ_R and Λ parameters can be expressed as [20]:

$$\sigma_R^2 = 1,23\, C_n^2 k^{7/6} L^{11/6} \tag{3}$$

$$\Lambda = \frac{2L}{k w_{ST}^2} \tag{4}$$

where k is the wave number of the laser beam and w_{ST} is the *short-term* beam radius at the receiver, which takes into account only spreading caused by small eddies (compared to the beam diameter), whereas the *long-term* beam radius takes into account also deflections from large eddies. If the next inequalities are satisfied:

$$\sigma_R^2 < 1 \tag{5}$$

and

$$\sigma_R^2 \cdot \Lambda^{5/6} < 1 \tag{6}$$

the scenario corresponds to weak fluctuations. On the contrary, if any of those conditions is not satisfied, the fluctuations are classified as moderate ($\sigma_R^2 \approx 1$) or strong ($\sigma_R^2 > 1$) conditions [20].

Some of the magnitudes described above, such as C_n^2 and σ_R^2, will be used to characterize the turbulence regime present in the experimental conditions of the tilt correcting system that will be described in section III and IV.

III. EXPERIMENTAL SETUP

Reducing solar background noise is an essential requirement for decreasing the QBER in free-space discrete- variable daylight QKD. One technique to achieve this is by reducing the receiver's field of view through active stabilization or tracking of the beam centroid. The purpose of a beam tracking system is thus reducing beam deviations caused by atmospheric beam wandering in a QKD receiver. The tracking system designed here was integrated in the receiver, which in many practical scenarios of distance and turbulent regime, is sufficient to increase the signal-to-noise ratio to the required levels

[1]The diameter of the receiver aperture must be considered in the denominator when the long-term beam diameter is equal or larger than the aperture On the contrary, if the long-term diameter is smaller than the receiver aperture, the long-term beam diameter should be considered instead of the receiver aperture.

of successful QKD [27]. Needless to say, these techniques must always been accompanied by both spectral filtering techniques of the quantum signal from the solar radiation and light-tight designs of both sender and receiver. Beam tracking techniques generally use an automated control that implements a proportional-integrative- derivative (PID) feedback loop between the beam position measured in a position sensitive detector (PSD) and an actuator, capable of deflecting the beam in order to correct for the deviations and provide a position where the error is minimized. If only one feedback loop in a close loop is used, beam deviations are corrected in a single point within a transverse plane of the receiver. This plane is usually the focal plane of the receiver in QKD systems, in order to minimize the field of view and thus the amount of solar background photons coupled into the detectors. This means the PSD in the control loop must be at an equivalent plane of the focal plane.

However, working in the focal plane is sometimes tricky for PSDs. On one hand, spot displacements in this plane are usually very small for lateral-effect PSDs to detect with sufficient SNR [28]. As for quadrant detectors (QDs), if the beam is too small it can fall into the gap or insensitive area where it cannot be detected, and in general, they are preferably used with lager beams to increase their linear region [28]. Furthermore, if the correction must be achieved in several planes of the quantum receiver where the detectors are placed, as it is the case in many QKD protocols, the QKD receiver must be carefully aligned to place all its detectors at exactly equivalent planes to that of the PSD. This implies not only placing them at the right equivalent plane but also ensuring the distance from the actuator to each lens preceding each detector is the same [27]. This can increase the complexity of the optical design.

On the other hand, designing a tracking system that includes two, instead ofone, correcting loops stabilizes the beam in two different points of the optical axis, thus making the beam stable in the whole receiver. This design removes the need to place the correcting detectors in the focal plane of the receiver, since *any* two planes can be used, as long as they are different spatial planes. The focal plane can now be avoided, if desired, facilitating the use of quadrant-type PSDs. The advantage of QDs is that they are cheap and off- the-shelf components, compared to, for example, high-frame rate CCD or CMOS cameras, and they do not require image- processing software, which can increase the complexity of beam acquisition. They also have good sensitivity (of a few μm and below), independent of the received optical power, and high bandwidth (MHz). As for the actuators, push-pull coils-based Fast Steering Mirrors (FSM) with a measured bandwidth of 500 Hz, sufficient to correct for beam wander effects, which are typically below 200 Hz, in the frequency spectrum, were selected.

Since the beam steering system was designed for a QKD system [29] that uses a 850 nm-wavelength signal for the quantum signal and a 1550 nm-wavelength signal for the timing synchronization signal, both of these wavelengths were

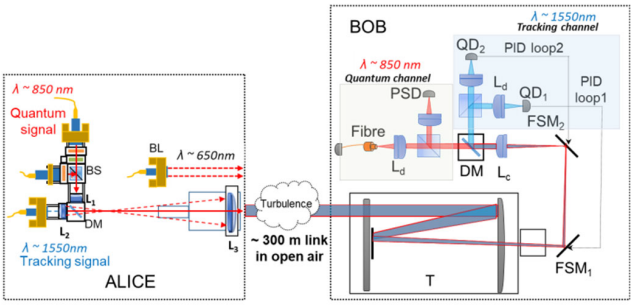

FIGURE 1. Experimental setup for characterizing wavefront tilt correction using single or double-loop correcting strategies. The transmitter sent two collimated and coincident 3.5-cm diameter beams at wavelengths of 1550 nm and 850 nm for the tracking and quantum signals, respectively. In the receiver one or two correcting loops composed of a Fast Steering Mirror (FSM) and a Quadrant Detectors (QD) were used to minimize deviations caused by atmospheric turbulence. The correction was monitored by a lateral-effect Position Sensitive Detector (PSD) and an optical fiber. (DM: Dichroic mirror; BL: Beacon laser; BS: 50/50 beamsplitter; L_c : 250 mm focal length collimating lens; L_d : 30 mm focal length detector lens; T: Schmidt-Cassegrain telescope).

used to characterize the performance of the tracking system. The 1550 nm-wavelength was used to perform the tracking, and the 850 nm-wavelength as the quantum signal over which the correction was observed and characterized.

In the transmitter (see Figure 1), the outputs of two fiber-coupled CW laser diode modules were collimated, combined and expanded by two $\times$ 5 beam expanders: L_1 and L_3 for the 850 nm-wavelength beam and L_2 and L_3 for 1550 nm-wavelength (focal lengths $f_1, f_2 = 60$ mm and $f_3 = 300$ mm) to obtain two identical 35 mm-diameter beams. They were then spectrally combined using a Dichroic Minor (DM) and mounted over a two-motor gimbal platform with two DC motors that provided elevation (RVS80) and azimuth (RV120) μrad-precision movements.

In the receiver, we used a 25.4-cm diameter LX200 Schmidt-Cassegrain telescope to collect both tracking and quantum signals, and a Dichroic Minor (DM) to spectrally discriminate them and direct them to their corresponding channels. Since the characterization of the performance of the correcting system was the main priority, the quantum channel was simplified by an optical fiber where the optical power coupled was recorded before and after correcting. A Silicon lateral-effect PSD 9 $\times$ 9 mm area, $f_{3\text{dB}} = 16$ KHz with a 55mV/μW responsivity was also employed to measure the beam position with and without correction. The transmitter and receiver were located at two different buildings separated by a distance of 300 meters in CSIC campus (see Figure 2). For simplicity purposes, we will refer to the lateral-effect PSD as simply PSD and to the quadrant detector PSD as simply QD.

The QDs were made of InGaAs with 3 $\times$ 3 mm area and a responsivity of 0.9 A/W (at 1.3 μm) and a $f_{3\text{dB}} = 15$MHz. The two control PID loops are each composed ofa FSM and a QD, and must be independent from each other. To achieve this, one of the QDs is placed in the image plane of the minor that is not connected to (in our case QD_1 is placed in the image

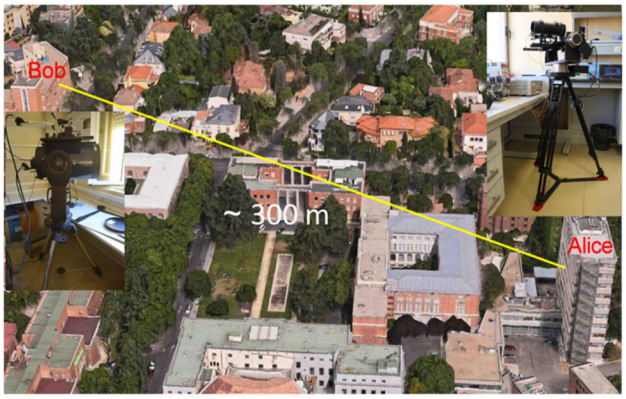

FIGURE 2. 300-meter link of between ICA-CSIC (Alice) and ITEFI-CSIC (Bob). Source: Google Ealth.

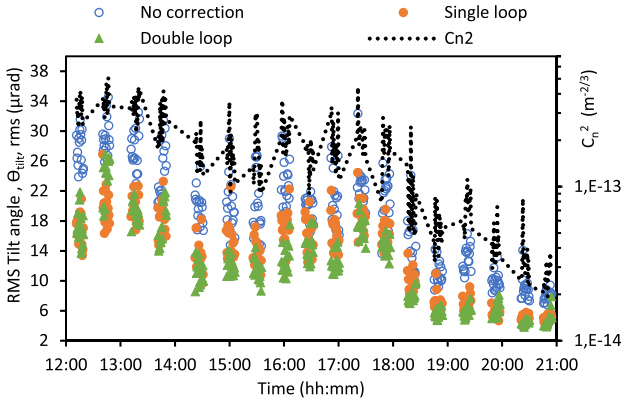

FIGURE 3. Experimental values of the tilt angle before and after correcting versus the time of the day measured on the 27th of July 2018 for the 300- metre link. Empty circle dots correspond to values with no correction applied; full circles to correction by single-loop; triangles to double-loop correction; and the dashed line to the refractive-index structure parameter, C_n^2 (represented in the secondary axis). Each point is the standard deviation of a 8-s measurement. Data was taken in series of16 measurements every 30 minutes during 9 hours. Sunset was at 21:34.

plane of FSM_2). Thus, QD_1 did not detect the movements of the beam due to the rotations of FSM_2, avoiding mechanical coupling between both actuators, which can turn the double-loop tracking system unstable. Furthermore, the response of both actuators was low-pass filtered around 200 Hz to ignore higher frequency atmospheric distortions, which also improved the stability of the system.

For comparison purposes, with each measurement of the correction by the system with two control loops, we also tested the correction using only one loop, by simply switching FSM_1 off and leaving FSM_2 ON. Therefore, QD_2 was placed at the focal plane of the detector, L_d, since this plane must be used when using only one correcting loop. The optical fibre and PSD at the observation channel were thus both placed at equivalent planes to that of QD_2, i.e., the focal plane of identical lenses L_d at each arm of the data channel.

IV. EXPERIMENTAL RESULTS

The method used to characterize the correcting strategies with one and two feedback loops consisted in measuring both the *rms* spot focal wander $\sqrt{\langle r_a^2 \rangle}$ (see section II) in the PSD and the optical power coupled in an optical fiber in the focal plane of the receiver. With these measurements, we calculated the *rms* tilt angle $\sqrt{\langle \theta_{tilt}^2 \rangle}$ and average coupling efficiency η, respectively, before and after correcting.

The measuring technique consisted in taking several sequences of data every hour for a total duration of 9 hours. This data were the spot position in the PSD and optical power at the fiber, with each sequence containing several intervals. The first interval was measured with the tracking system turned OFF, the next interval with one correcting loop turned ON (single-loop strategy), and the latest with the two correcting loops ON (double-loop strategy). Each sequence was taken every 30 minutes and consisted of 5 series of intervals with an interval duration of 30 seconds, followed by 16 series of intervals with interval duration of 8 seconds. The different duration was chosen to study the dependence of the measured values with the time interval finding out that similar results were achieved for both time durations.

The sampling rate for the centroid position from the PSD was 4000 Hz (using a DAQ USB-6343 from NI). For the fiber coupling efficiency the maximum sample rate that could be achieved was of 2 Hz from acquisition limitations of the equipment (PM200). However, as previously stated, data was taken in sufficiently long time intervals to be statistically significant in both cases.

A. IMPROVEMENT IN TILTANGLE AFTER CORRECTION

The performance ofboth beam-tracking techniques using one and two correcting loops was characterized in a 9-hour experiment for a distance of 300 meters and it is shown in Figure 3.

The improvement factor, (ratio of the tilt angle after correcting to the value before correcting) was evaluated for both type of correction strategies. A maximum improvement factor of 2.3 for the single-loop strategy and 2.9 for the double-loop strategy were found, whereas the average value for the whole 9 h-measurement was 1.5 for the former strategy and 1.8 for the latter. This meant that with the double-loop strategy the improvement factor was up to a 20-25% better than for the single loop. According to our simulations this is due to the minimization of optical aberrations in the double-loop strategy compared to single loop one. The reason for this is that the beam is forced to pass as close as possible to the center of the optical lenses in Bob, reducing the effect of aberrations such as spherical or coma, which are proportional to the distance from the center of the lens to the point of beam incidence. A theoretical model was studied in [30] to assess the quality of the experimental correction and was found to be in very good agreement with the theory. The refractive index structure parameter C_n^2 was calculated from the experimental values of r_a using equations (1) and (2) and they were found to be ranging from moderate ($C_n^2 - 10^{-14}\mathrm{m}^{-2/3}$) to strong ($C_n^2 - 10^{-13}\mathrm{m}^{-}2/3$) turbulent regimes. Since only tilt aberrations are corrected, and not higher orders modes,

the amount of uncorrected aberrations in the wavefront can be expressed as a residual error, which in the case oftilt correction is of order three, and can be expressed as [26]:

$$\Delta_3 = 0.134\,(2w_G/r_0)^{5/3} \tag{7}$$

where $2w_G$ is the diameter of the receiver aperture, and r_0 is the Fried parameter, defined by [20]:

$$r_0 = 1,67\left(C_n^2 L k^2\right)^{-3/5} \tag{8}$$

This residual error, Δ_3, increases with the turbulent regime C_n^2 and the distance of the link, L, as can be deduced from equations (7) and (8), which explain *s* the increase of both corrected and no corrected values of θ_{tilt} when the turbulence gets stronger (see Figure 3).

If θ_{tilt} is reduced with the correction, then the field of view of the receiver can be reduced accordingly, and with it, the solar background noise that enters this field of view. The QBER can be expressed as two terms [31]:

$$QBER = \kappa + \frac{D}{2B} \tag{9}$$

A constant term κ, due to imperfections of the QKD system, and a second term given by the probability of a dark, or solar background photon, to be detected. The reduction in the QBER contribution caused by solar photons can then be expressed as:

$$\frac{QBER_{\text{after}}}{QBER_{before}} = \frac{(D/2B)_{after}}{(D/2B)_{before}} = \frac{D_{after}}{D_{before}} \tag{10}$$

where B is the *sifted bit rate* at Bob, D is the number of photons from solar background per unit time and the subindexes *before* and *after* refer to before and after correcting the tilt of the wavefront. We assume B the same ifbefore and after correcting we choose an optical fiber as large as the maximum area of the long-term beam. Since D is actually the background *photon flux*, $\emptyset$, equation (10) can be expressed as:

$$\frac{QBER_{after}}{QBER_{before}} = \frac{\phi_{after}}{\phi_{before}} = \frac{(I \cdot A/\hbar\omega)_{after}}{(I \cdot A/\hbar\omega)_{before}} = \frac{A_{after}}{A_{before}} \tag{11}$$

where I and ω are the intensity and angular frequency, respectively, of the beam entering the field of view of area A at the receiver. Since the intensity and angular frequency of the beam is equal before and after correcting, the reduction of the QBER is a function of only the area ofbeam fluctuations before and after correcting. This means the QBER is decreased quadratically with the reduced focal spot wander r_a, which in turn, is proportional to θ_{tilt}. The reduction in the QBER was then estimated from the experimental values measured of the θ_{tilt} before and after correcting at 300 meters for both strategies and the results can be seen in Figure 4. The QBER was decreased by 82% for the single-loop strategy and 88% for the double-loop strategy. The main results are shown in Table 1.

The performance of the double-loop strategy was also compared through the Probability Density Function (PDF) of the tilt angle under different turbulence fluctuations, given by the Rytov parameter. Data in the top of Figure 5 corresponds to a regime of strong fluctuations, whereas the figures below correspond to weak to moderate fluctuations regimes.

The PDF's width decreases after correction for the whole range between weak to strong fluctuations. It can be observed from the histograms that the broadening of the corrected signal increases with the strength of the turbulent regime but a 1.6 improvement factor can still be achieved in strong turbulent regime (top left of figure 5).

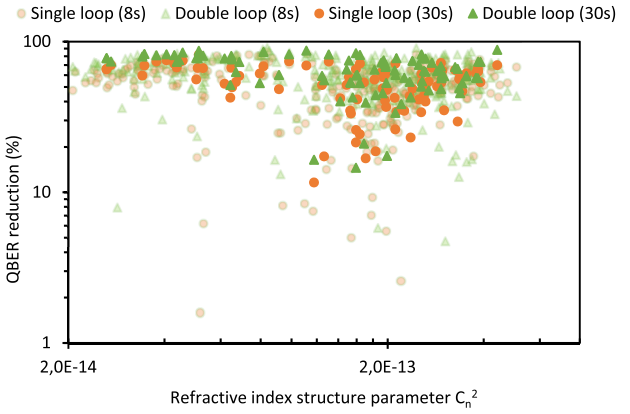

FIGURE 4. Reduction in the QBER (%) contribution due to solar background noise after correcting with single and double-loop strategies as a function of the measured refractive index structure parameter. Measurements were taken for 9 hours and each (semitransparent) solid point corresponds to a measurement of (8) 30 seconds.

TABLE 1. Improvement factors (IF) for the single and double-loop correcting strategies for the best and average values of the correction obtained during a 9-hour experiment at 300-meters link.

	Single loop		Double loop	
	IF	Decrease in $QBER_{bckg}$ (%)	IF	Decrease in $QBER_{bckg}$ (%)
Best correction	2,3	81,6	2,9	88,0
Average correction	1,5	55,7	1,8	68,7

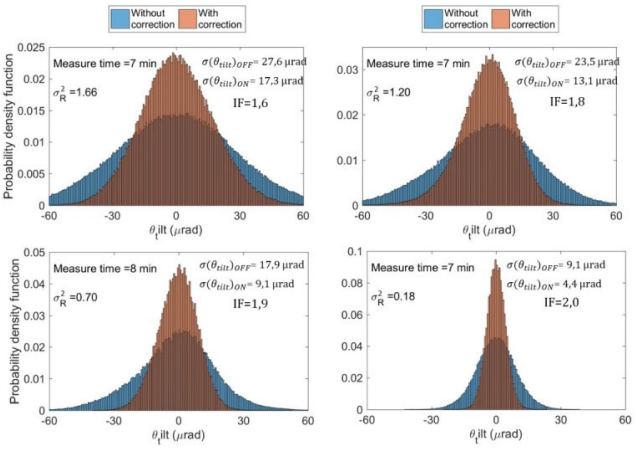

FIGURE 5. Probability density function (PDF) of the tilt angle before and after correcting for several turbulent fluctuations measured in a 300-m free- space link. The values of the tilt angle are given as the standard deviation of the distribution (σ) and the improvement factor (IF) values are also shown.

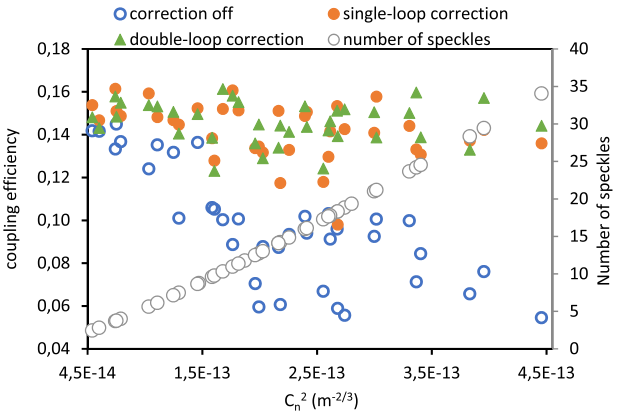

FIGURE 6. Coupling efficiency in 9.5μm core-diameter single-mode fiber before and after correction with single and double-loop beam tracking strategies for a free-space 300 m link. Number of speckles is also shown in the secondary axis. Data was taken on the 27/07/2018 for 9 hours and each point corresponds to a measurement of 30 seconds.

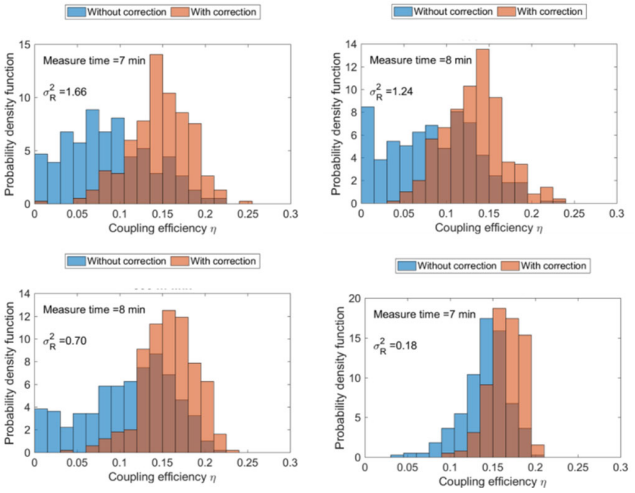

FIGURE 7. Coupling efficiency measured in 9.5μm core-diameter single-mode fiber for 300-meter link and different values of the turbulent regime characterized by the Rytov parameter. Measurements were taken for 7 to 8 minutes before and after correcting with the double-loop strategy. Similar results were obtained for the single-loop strategy.

B. IMPROVEMENT IN OPTICAL FLBER COUPLING EFFICIENCYAFTER CORRECTION

Monitoring the correction of the tracking system in optical fiber is also relevant since most QKD systems use them as spatial filtering and guiding mechanism to the single photon detectors. The selection on the type of fiber (multimode or single mode) depends on the characteristics of the application. Multimode fiber might be more adequate in applications where the received signal (the quantum key) must be simply stored, whereas single mode (standard telecommunication) fiber might be more convenient when the received signal is to be routed into a communication network where fiber-optic communications components are built in SMF fiber (e.g. erbium-doped fiber amplifiers). In this case, the receiver unit can be seen as a relay or intermediate station that interconnects a free-space link and an optical fiber network.

We therefore used two types of optical fibers: a SMF and multimode fiber in the receiver to observe the correction by measuring the coupling efficiency η, before and after correcting:

$$\eta = \frac{P_f}{P_i} \tag{12}$$

where P_f is the coupled optical power at the fiber end in the receiver, and P_i is the input optical power before the fiber (see Figure 2). The fiber coupling efficiency for each fiber was then measured in a 9-hour experiment and represented against the turbulent strength characterized by C_n^2, as shown in figure 6. This time, the difference in performance from the double-loop to the single-loop strategies cannot be observed due to the lower sensitivity of the coupling efficiency measurement, which is limited by diameter of the fiber, and this is larger than the quadrant and lateral-effect detectors' sensitivity ($< \mu$rad), used in previous measurements. The improvement factor in the coupling efficiency in SMF after correction increased with the turbulent regime reaching a factor of2.5 for high values of C_n^2 where the range for correction is larger. For the measurements taken in this work, fluctuation regimes ranged from a Rytov parameter of 0.15 to 2.28, classified as to weak to strong fluctuations regime, while C_n^2 ranged from 2. 6.10$^-$ 14-2/3 m up to 4. 4.10^{-13}m$^{-2/3}$. The number of speckles, which is a measure of the coherence of the beam, is also plotted in Figure 6. This number is given by A_r/A_ρ, where A_r is the area of the receiver aperture and A_ρ is the coherence area, given by $A_\rho = \pi\rho_{c^2}$. The spatial coherence length ρ_c is twice the Fried parameter r_0, given in equation (8). It can be observed that the coupling efficiency decreases rapidly with the number of speckles.

A further analysis of the system performance in terms of coupling efficiency for different turbulence regimes through the probability density function (PDF) was also carried through. The power coupled in the SMF before and after correction is shown in Figure 7 for several values of the turbulent regime. The width of the PDF is decreased and its height displaced to the right, which means the coupling efficiency is improved after correction.

A multimode fiber was also used to compare the performance of the correcting system in terms of coupling efficiency (see Figure 8). We used a relatively small diameter fiber $of 25 - \mu$m core-diameter fiber, since it was more suitable for the amount of turbulence present in the characterized link (300m) than a fiber with a larger core diameter (50μm or 62.5 μm), which might have been too large to observe significant differences before and after correcting. Once the coupling efficiency was measured, the QBER was estimated from the experimental values for each fiber.

An improvement factor in the coupling efficiency of more than two after correcting was measured for both types of fibers and correcting strategies. This causes a reduction in the QBER of more than 50%, which can be deduced

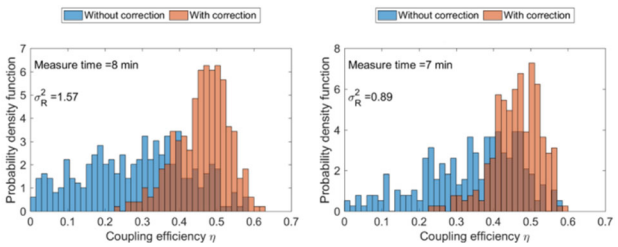

FIGURE 8. Coupling efficiency measured in 25μm core-diameter single-mode fiber for 300-meter link and different values of the turbulent regime, characterized by the Rytov parameter. Measurements were taken for 7 to 8 minutes before and after correcting with the double-loop strategy. Similar results were obtained for the single-loop strategy.

TABLE 2. Improvement factor and reduction in QBER in single mode telecommunication fiber and 25μm core diameter fiber after tilt correction with two correcting loops for a 300 m link.

Improvement factor in coupling efficiency			Reduction in $QBER_{bckg}$ (%)
9.5 µm-core diameter fiber (SMF)	maximum value	2,1	52,3
	average value	1,5	34,8
	maximum value @ $C_n^2 = 10^{-13}$ ($m^{-2/3}$)	2,1	52,3
	average value @ $C_n^2 = 10^{-13}$ ($m^{-2/3}$)	1,7	42,5
	maximum value @ $C_n^2 = 10^{-14}$ ($m^{-2/3}$)	1,1	9,4
	average value @ $C_n^2 = 10^{-14}$ ($m^{-2/3}$)	1,1	6,9
25 µm-core diameter fiber	maximum value	1,6	38,7
	average value	1,6	35,8
	maximum value @ $C_n^2 = 10^{-13}$ ($m^{-2/3}$)	2,0	50,2
	average value @ $C_n^2 = 10^{-13}$ ($m^{-2/3}$)	1,4	30,2
	maximum value @ $C_n^2 = 10^{-14}$ ($m^{-2/3}$)	2,1	52,3
	average value @ $C_n^2 = 10^{-14}$ ($m^{-2/3}$)	1,6	37,5

from equations (*9*) and (*10*). The increase in coupling efficiency for one particular fiber means the bit rate received in Bob, B, increases by the same factor, whereas D remains constant. A summary of the improvement factors after correcting with the double-loop strategy for both fibers taken for 9 hours and the effect in the QBER is shown in Table 2.

It can be seen from table 2 that the improvement in coupling efficiency after correction is translated into a reduction in the QBER of more than 50% for the SMF fiber and almost 40% for the 25 $-$ μm core-diameter fiber. For the scenarios with stronger turbulence, the reduction is stronger as more range for correction is available.

TABLE 3. Parameters of the theoretical model from left to right: Transmitter's clock frequency, R(GHz); mean photon number per pulse, μ; Alice's aperture diameter[2], DA (mm); atmospheric transmittance, T_a (km); Bob's aperture diameter, DB (mm); Bob's transmittance, T_B; B92 protocol's transmittance, T_{B92}; detector's transmittance, T_{Det}; detector's dark count rate, $D(s^{-1})$; efficiency of error correcting protocol, $f(e)$; constant fraction of the quantum bit error rate, k; and fraction of the quantum bit error rate caused by solar photons, e_{bckg}.

R	µ	D_A	T_a	D_B	T_B	T_{B92}	T_{Det}	D	f(e)	κ	e_{bckg}
1.5	0.1	35	0.62	80	0.19	0.25	0.3	250	1.1	0.02	0.04

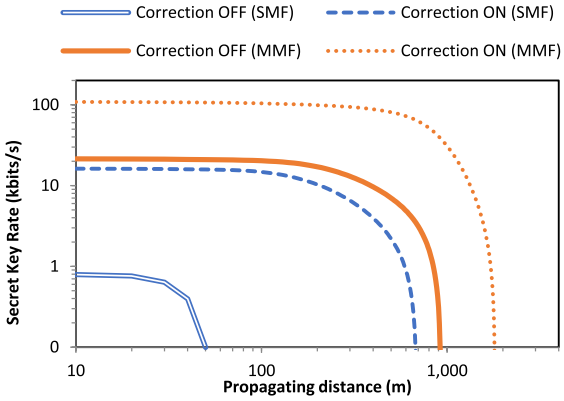

FIGURE 9. Theoretical secret key rate versus propagating distance before and after correcting for a strong turbulence regime ($C_n^2 = 10^{-13}m^{-2/3}$) and daylight conditions ($e_{bckg} = 0.04$) for single and multimode fibers with core diameters 9.5 μm and 25 μm, respectively.

The secret key rate, R_{secret}, (bits /s) for the QKD system in [29] was theoretically calculated using:

$$R_{secret} = R_{sifted}\left[(1 - I_{AE}) - f(e)H_2(e) - (1 - I_{AE})H_2\left(\frac{e}{1-I_{AE}}\right)\right] \quad (13)$$

where I_{AE} is the maximum information shared by Alice and Eve, $f(e)$ is the efficiency of the error correcting algorithm, H_2 is the binary entropy function and e is the total QBER. Assuming that a Unambiguous State Discrimination (USD) [32] attack is taking place, I_{AE} is given by $I_{AE} = 1 - \cos\theta$, with θ being the angle between the two polarized states, and equal to 45°. The SKR was calculated with and without the maximum improvement factor in the coupling efficiency (a factor -2) for both the SMF and MMF fibers in strong turbulence regime ($C_n^2 = 1 \times 10^{-13}m^{-2/3}$) and daylight conditions (solar QBER contribution of 4%). The remaining parameters were chosen similar to those in [28]:

The increase in R_{secret} is due to both the increase in R_{sifted} and the decrease in the QBER caused by the improvement in the coupling efficiency with correction. Additionally, the increase in R_{secret} after correcting is more noticeable for smaller core-diameter fibers, since the range for improvement

[2]For simplicity, a receiver aperture of 80 mm in diameter was considered, since this is the maximum circular clear aperture when the beam is pointed off center and to the side strip of the telescope.

after correction is larger. This improvement is more than one order of magnitude for the SMF and a factor of five for the MMF. On the other hand, the maximum distance of the QKD link increases from only 50 meters without correction to 680 meters for the SMF when the correction is applied, and from 900 meters to 1800 meters in the case of the MMF.

V. CONCLUSION AND FUTURE WORK

Atmospheric wavefront tilt correction is essential to achieve successful QKD in free-space links. We have presented a tilt correcting system with a double control loop. This system stabilizes the beam in the whole optical axis instead ofa single plane, removing the need of placing the single-photon detectors in equivalent planes to the PSD detector used in the correcting loop. Despite using two control loops, the system is stable and achieves a better improvement factor, in reducing beam fluctuations in the focal plane of the receiver, than a single-loop system (2.9 compared to 2.3 for the best correction achieved).

The coupling efficiency measured in both a SMF and a multimode $25-\mu$m core diameter optical fibers increased more than a factor oftwo with the correction applied, which reduces more than 50% the main contribution to the QBER in free- space QKD systems, which is caused by solar background photons. Moreover, this implies an increase in the secret key rate of more than one order of magnitude in strong turbulent regimes and daylight conditions when using a single mode fiber, and a factor of five in the case of a multimode ($25-\mu$m core diameter) fiber. This correcting system can therefore help improve the connectivity of free-space to fiber-optic telecommunication networks for the case of SMF results. For the case of multimode fiber results, the correcting system improves the signal to noise ratio in the receiver when no connection to preinstalled fiber networks is present. Furthermore, the correcting system was implemented using cheap and off-the-shelf components, suitable for compact and commercial metropolitan QKD systems, and the achieved correction was present even under strong turbulence regimes ($C_n^2 \sim 10^{-13}\mathrm{m}^{-2/3}$).

REFERENCES

[1] E. Diamanti, H. Lo, B. Qi, and Z. Yuan, "Practical challenges in quantum key distribution," *NPJ Quantum Inf.*, vol. 2, Nov. 2016, Art. no. 016025.

[2] D. Huang, "Continuous-variable quantum key distribution with 1 Mbps secure key rate," *Opt. Express*, vol. 23, no. 13, pp. 17511–17519, 2015.

[3] S. Bahrani, M. Razavi, and J. A. Salehi, "Orthogonal frequency-division multiplexed quantum key distribution," *J. Lightw. Technol.*, vol. 33, no. 23, pp. 4687–4698, Dec. 1, 2015.

[4] G. Vest, M. Rau, L. Fuchs, G. Corrielli, H. Weier, S. Nauerth, A. Crespi, R. Osellame, and H. Weinfurter, "Design and evaluation of a handheld quantum key distribution sender module," *IEEE J. Sel. Topics Quantum Electron*, vol. 21, no. 3, May/Jun. 2014, Art. no. 6600607.

[5] C. Ma, W. D. Sacher, Z. Tang, J. C. Mikkelsen, Y. Yang, F. Xu, T. Thiessen, H.-K. Lo, and J. K. S. Poon, "Silicon photonic transmitter for polarization-encoded quantum key distribution," *Optica*, vol. 3, no. 11, pp. 1274–1278, 2016.

[6] P. Sibson, C. Erven, M. Godfrey, S. Miki, T. Yamashita, M. Fujiwara, M. Sasaki, H. Terai, M. G. Tanner, C. M. Natarajan, R. H. Hadfield, J. L. O'Brien, and M. G. Thompson, "Chip-based quantum key distribution," *Nature Commun.*, vol. 8, p. 13984, Feb. 2017.

[7] H. Ko, J.-S. Choe, B.-S. Choi, K.-J. Kim, J.-H. Kim, Y. Baek, and C. J. Youn, "Daylight operation of a high-speed free-space quantum key distribution using silica-based integration chip and micro-optics-based module," in *Proc. Opt. Fiber Commun. Conf. Exhib. (OFC)*, Mar. 2019, pp. 1–3.

[8] R. Ursin, F. Tiefenbacher, T. Schmitt-Manderbach, H. Weier, T. Scheidl, M. Lindenthal, B. Blauensteiner, T. Jennewein, J. Perdigues, P. Trojek, B. Ömer, M. Fürst, M. Meyenburg, J. Rarity, Z. Sodnik, C. Barbieri, H. Weinfurter, and A. Zeilinger, "Entanglement-based quantum communication over 144 km," *Nature Phys.*, vol. 3, pp. 481–486, Jun. 2007.

[9] S.-K. Liao, H. L. Yong, C. Liu, G. L. Shentu, D. D. Li, J. Lin, H. Dai, S. Q. Zhao, B. Li, J. Y. Guan, and W. Chen, "Long-distance free-space quantum key distribution in daylight towards inter-satellite communication," *Nature Photon.*, vol. 11, no. 8, pp. 509–513, 2017.

[10] Y.-H. Gong, K.-X. Yang, H.-L. Yong, J.-Y. Guan, G.-L. Shentu, C. Liu, F.-Z. Li, Y. Cao, J. Yin, S.-K. Liao, J.-G. Ren, Q. Zhang, C.-Z. Peng, and J.-W. Pan, "Free-space quantum key distribution in urban daylight with the SPGD algorithm control of a deformable mirror," *Opt. Express*, vol. 26, no. 15, pp. 18897–18905, 2018.

[11] M. Fujiwara, T. Ito, M. Kitamura, H. Endo, O. Tsuzuki, M. Toyoshima, H. Takenaka, Y. Takayama, R. Shimizu, M. Takeoka, R. Matsumoto, and M. Sasaki, "Free-space optical wiretap channel and experimental secret key agreement in 7.8 km terrestrial link," *Opt. Express*, vol. 26, no. 15, pp. 19513–19523, 2018.

[12] S. Nauerth, F. Moll, M. Rau, C. Fuchs, J. Horwath, S. Frick, and H. Weinfurter, "Air-to-ground quantum communication," *Nature Photon.*, vol. 7, pp. 382–386, Mar. 2013.

[13] J. Wang, "Direct and full-scale experimental verifications towards ground–satellite quantum key distribution," *Nature Photon.*, vol. 7, pp. 387–393, Apr. 2013.

[14] A. D. Hill, J. Chapman, K. Herndon, C. Chopp, D. J. Gauthier, and P. Kwiat, "Drone-based quantum key distribution," in *Proc. QCrypt Conf.*, Sep. 2017.

[15] H. Takenaka, A. Carrasco-Casado, M. Fujiwara, M. Kitamura, M. Sasaki, and M. Toyoshima, "Satellite-to-ground quantum-limited communication using a 50-kg-class microsatellite," *Nature Photon.*, vol. 11, pp. 502–508, Jul. 2017.

[16] S.-K. Liao, W. Q. Cai, W. Y. Liu, L. Zhang, Y. Li, J. G. Ren, J. Yin, Q. Shen, Y. Cao, Z. P. Li, and F. Z. Li, "Satellite-to-ground quantum key distribution," *Nature*, vol. 549, no. 7670, pp. 43–47, Sep. 2017.

[17] J.-G. Ren, P. Xu, H. L. Yong, L. Zhang, S. K. Liao, J. Yin, W. Y. Liu, W. Q. Cai, M. Yang, L. Li, and K. X. Yang, "Ground-to-satellite quantum teleportation," *Nature*, vol. 549, pp. 70–73, Sep. 2017.

[18] S.-K. Liao, W. Q. Cai, J. Handsteiner, B. Liu, J. Yin, L. Zhang, D. Rauch, M. Fink, J. G. Ren, W. Y. Liu, and Y. Li, "Satellite-relayed intercontinental quantum network," *Phys. Rev. Lett.*, vol. 120, Jan. 2018, Art. no. 030501.

[19] M. Sasaki, "Quantum networks: Where should we be heading," *Quant. Sci. Tech.*, vol. 2, no. 2, Apr. 2017, Art. no. 020501.

[20] L. C. Andrews and R. L. Phillips, *Laser beam propagation through random media*. Bellinngham, WA, USA: SPIE Optical Engineering Press, 2005.

[21] I. Capraro, A. Tomaello, A. Dall'Arche, F. Gerlin, R. Ursin, G. Vallone, and P. Villoresi, "Impact of turbulence in long range quantum and classical communications," *Phys. Rev. Lett.*, vol. 109, Nov. 2012, Art. no. 200502.

[22] M. R. Suite, H. R. Burris, C. I. Moore, M. J. Vilcheck, R. Mahon, C. Jackson, M. F. Stell, M. A. Davis, W. S. Rabinovich, W. J. Scharpf, A. E. Reed, and G. C. Gilbreath, "Fast steering mirror implementation for reduction of focal-spot wander in a long-distance free-space optical communication link," *Proc. SPIE*, vol. 5160, pp. 439–446, Jan. 2004.

[23] Y. Ni, J. Wu, X. San, S. Gao, S. Ding, J. Wang, and T. Wang, "Deflection angle detecting system for the large-angle and high-linearity fast steering mirror using quadrant detector," *Proc. SPIE*, vol. 57, no. 2, Feb. 2018, Art. no. 024110.

[24] T. Weyrauch and M. A. Vorontsov, "Atmospheric compensation with a speckle beacon in strong scintillation conditions: Directed energy and laser communication applications," *App. Opt.*, vol. 44, no. 30, pp. 6388–6401, 2005.

[25] M. T. Gruneisen, M. B. Flanagan, and B. A. Sickmiller, "Modeling satellite-Earth quantum channel downlinks with adaptive-optics coupling to single-mode fibers," *Proc. SPIE*, vol. 10442, Oct. 2017, Art. no. 104420E.

[26] R. J. Noll, "Zernike polynomials and atmospheric turbulence," *J. Opt. Soc. Amer.*, vol. 66, no. 3, pp. 207–211, 1976.

[27] A. Carrasco-Casado, N. Denisenko, and V. Fernandez, "Correction of beam wander for a free-space quantum key distribution system operating in urban environment," *Proc. SPIE*, vol. 53, no. 8, 2014, Art. no. 084112.
[28] V. Fernandez, J. Gómez-García, A. Ocampos-Guillén, and A. Carrasco-Casado, "Correction of wavefront tilt caused by atmospheric turbulence using quadrant detectors for enabling fast free-space quantum communications in daylight," *IEEE Access*, vol. 6, pp. 3336–3345, 2018.
[29] M. J. García-Martínez, N. Denisenko, D. Soto, D. Arroyo, A. B. Orue, and V. Fernandez, "High-speed free-space quantum key distribution system for urban daylight applications," *App. Opt.*, vol. 52, no. 14, pp. 3311–3317, 2013.
[30] P. Arteaga-Díaz, A. Ocampos-Guillén, and V. Fernandez, "Enabling QKD under strong turbulence for wireless networks with tilt wavefront correction," in *Proc. 21st Int. Conf. Transparent Opt. Netw. (ICTON)*, Angers, France, Jul. 2019, pp. 1–4.
[31] P. D. Townsend, "Quantum cryptography on optical fiber networks," *Opt. Fiber Technol.*, vol. 4, no. 4, pp. 345–370, Oct. 1998.
[32] K. Tamaki, M. Koashi, and N. Imoto, "Security of the Bennett 1992 quantum-key distribution protocol against individual attack over a realistic channel," *Phys. Rev. A, Gen. Phys.*, vol. 67, Mar. 2003, Art. no. 032310.

ALEJANDRO OCAMPOS-GUILLÉN graduated in physics from the Autonomous University of Madrid, in 2016. He received the M.S. degree in new technologies for electronics and photonics from the Complutense University of Madrid, in September 2017.

He completed his master's thesis with the Institute of Physical and Information Technologies (ITEFI), CSIC, where he was a Research Assistant, from October 2017 to March 2019. He was a beneficiary of a contract awarded by the Youth Employment Initiative (YEI) and the Operational Programme of Youth Employment, and funded by the European Social Fund.

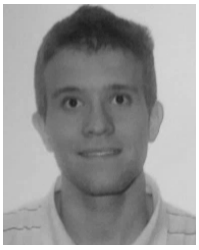

JORGE GÓMEZ-GARCÍA graduated in physics from the Complutense University of Madrid, in 2014. He received the M.S. degree in photonics from the Polytechnic University of Catalonia, in 2015.

From February 2016 to February 2018, he was a Research Assistant with the Institute of Physical and Information Technologies (ITEFI), CSIC, Madrid. He was a beneficiary of a contract awarded by the Youth Employment Initiative (YEI) and Operational Programme of Youth Employment, and funded by the Community of Madrid and the European Social Fund.

NATALIA DENISENKO received the B.S. degree in electrical and electronic engineering from the Moscow Power Engineering Institute, in 1975. She was with the Laser Physics Laboratory, Paris University, France, from 1975 to 1977, with the Materials Physics Institute, Spanish National Research Council, Madrid, Spain, from 1979 to 1982, and with the Ultrasonic and Acoustic Technologies Laboratory, National Research Council, Rome, Italy, from 1982 to 1985. In 1986, she joined the Spanish National Research Council.

VERONICA FERNANDEZ received the B.Sc. degree (Hons.) in physics with electronics from the University of Seville, in 2002, and the Ph.D. degree in physics from Heriot-Watt University, Edinburgh, U.K., in 2006, with title Gigahertz Clocked Point-to-Point and Multi-User Quantum Key Distribution Systems. She joined the Institute for Physical and Information Technologies, Spanish National Research Council (CSIC), Madrid, in November 2007, with a Postdoctoral Juan de la Cierva contract. In 2009, she received a permanent position at CSIC. Her main research interests include experimental high-speed quantum key distribution systems, both in free space and optical fiber, as well as laser-beam stabilization systems for correcting atmospheric turbulent effects in optical and quantum communications.